Laser-Driven Magnetized Liner Inertial Fusion on OMEGA

Introduction

Magnetized liner inertial fusion (MagLIF) is a concept that utilizes pulsed-power–driven Z pinches of metal liners to compress deuterium–tritium (DT) gas to fusion-relevant temperatures and pressures.[1] For cylindrical compression and pulsed-power time scales (~100 ns), it is required that the fuel be preheated to ~100 eV and axially magnetized to suppress radial conduction losses to achieve near-adiabatic compression, reducing the radial convergence required to reach the temperatures and pressures needed for thermonuclear fusion. At stagnation, the axial magnetic field is compressed to the point where it is strong enough to magnetize alpha particles,[2] allowing self-heating to occur at low areal densities.

Cylindrical implosions can be achieved with 40 beams of the OMEGA Laser System, and in fact, magnetized cylindrical implosions have been carried out on OMEGA,[3,4] leaving only the laser preheating of the gas. A single beam has been redirected down a symmetry axis of OMEGA to heat the gas prior to compression.

MagLIF is being scaled down from a pulsed-power–driven device to a laser-driven device for several reasons: pulsed-power devices, like the Z machine at Sandia National Laboratories, are very violent environments in terms of debris and electromagnetic noise, making it very difficult to field diagnostics and maintain a high shot rate. Furthermore, diagnostic access around the target chamber in Z is limited by the installation of the axial magnetic field coils and the geometry of the current delivery system. OMEGA can perform roughly 10× more shots per day than Z and can provide better statistics and wider scans of the MagLIF parameter space. Furthermore, OMEGA has the capability to perform measurements that cannot be done on the Z machine, such as proton radiography of the compressed axial magnetic field, low-yield neutron measurements, and time-resolved x-ray measurements of the liner trajectory. Experiments at the OMEGA scale can provide another experimental data point for the energy scaling of the MagLIF concept and will ultimately give us the confidence in extrapolating MagLIF to ignition-scale designs.

This article is a brief overview of the work done to establish a science platform for studying the physics of MagLIF on OMEGA. Future more-detailed papers will describe the separate steps taken to achieve this goal. The following sections present (1) a review of 1-D magnetohydrodynamic (MHD) results that were used to design the platform; (2) preliminary results from experiments conducted to achieve the required preheat and uniform cylindrical compression; (3) the first results from a fully integrated MagLIF implosion on OMEGA; and (4) future projects to be explored using this recently established experimental platform.

Point Design

The OMEGA point design[5] is energy scaled from the Z machine's 29-MA point design.[1] The conserved quantity is energy per unit volume, which mandates that the linear dimensions be scaled down by a factor of 10 to match the factor-of-1000 difference in driver energy between OMEGA and Z. Other factors such as fuel preheat and initial axial magnetic field can be the same. A higher implosion velocity will be needed at the OMEGA scale to compensate for increased thermal losses at the smaller scale. The preheat temperature, liner aspect ratio, and fuel density can be changed to achieve different implosion energetics for a complete scan of the MagLIF parameter space. An ensemble of 1-D MHD simulations that include electrothermal terms in Ohm's Law[6] was used to determine the optimal laser pulse length, taking into account the drop in on-target energy for pulses longer than 1 ns, and fuel density for shell thicknesses from 20 μm to 50 μm for a fixed 10-T initial axial magnetic field and 200-eV preheat temperature, the objective being to maximize neutron yield at a fuel convergence ratio close to the 25 chosen for the Z point design. Only a square-shaped laser pulse was considered. The optimal design for a 30-μm shell is a 1.5-ns pulse length with an initial fuel density >1.5 mg/cm^3 as shown in Fig. 150.1. Thicker shells did not give adequate final fuel temperatures.

This optimal point is for a fixed magnetic field and preheat temperature, which is easily achievable. If the magnetic-field capabilities of OMEGA are expanded to values above 10 T,

the optimal point may change. Increasing magnetic field and preheat reduces convergence ratio and implosion speed, providing a more stable cylindrical implosion. Higher core pressures are achieved for higher magnetic fields because of the suppression of radial conduction losses (seen in Fig. 150.2). A higher preheat temperature leads to a lower final pressure for a fixed energy implosion, which is consistent with a simple model for adiabatic compression. For a given energy in a piston E and initial pressure P_0 and volume V_0, the final pressure increase is

$$\frac{P_f}{P_0} = \left(\frac{E}{P_0 V_0}\right)^{\gamma/\gamma-1} \tag{1}$$

and is therefore inversely proportional to the starting temperature for a fixed initial mass piston. Substituting this back into the energy balance equation and solving for the convergence ratio, we obtain

$$\mathrm{CR} = \frac{R_0}{\sqrt{E/P_f \pi}}, \tag{2}$$

which is proportional to the final pressure or inversely proportional to the initial temperature. Higher starting temperatures, therefore, give a lower final pressure and lower convergence ratio, which is the trend highlighted in Fig. 150.2.

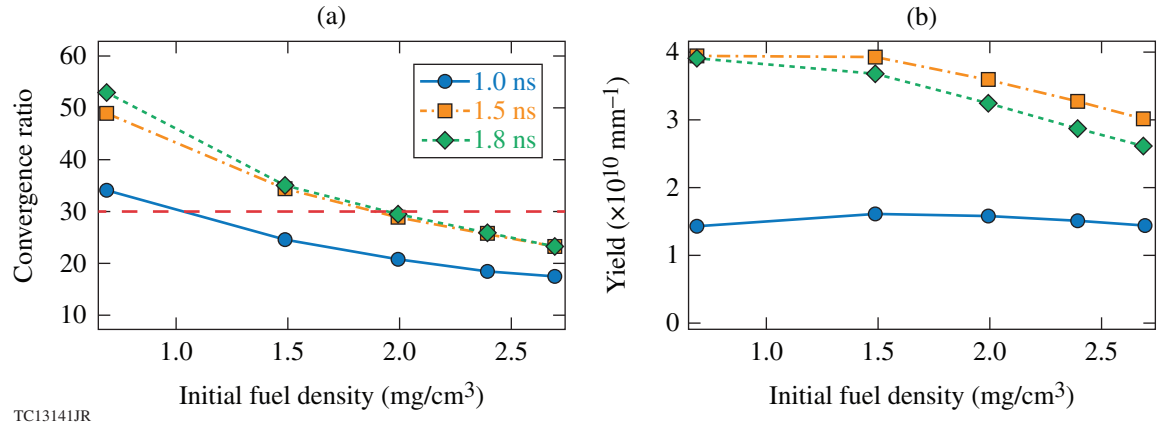

Figure 150.1
(a) The D_2 fuel convergence ratio as a function of initial gas density for three different pulse lengths; (b) the neutron yields from each of these designs. These plots show that a 1.5-ns pulse is optimal and that the design requires an initial fuel density higher than that which optimizes neutron yield to maintain a fuel convergence ratio <30, indicated by the red dashed line.

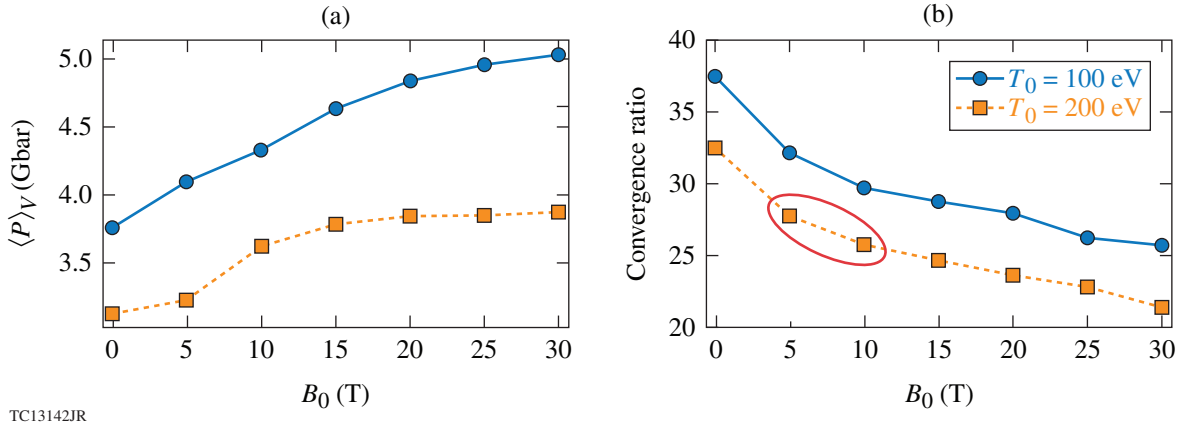

Figure 150.2
(a) As the magnetic field increases, the volume-averaged thermal pressure of the fuel increases, resulting in (b) a lower convergence ratio at the end of the implosion. This is mostly caused by the magnetic field suppressing radial conduction losses. The red circled region is the point design considering the capabilities of the OMEGA Laser System.

Regardless of the starting magnetic field or shell thickness, 1-D calculations show that a minimum preheat temperature of ~100 eV is required for neutron yield increases larger than a factor of 2 from the magnetic field above the implosion-only baseline of $\sim 10^{10}$ mm^{-1}. Once above the threshold preheat, neutron yields and ion temperatures do not increase with initial temperature, but convergence ratio decreases, increasing the stability of the imploding shell. With a sufficient preheat temperature, increasing the initial magnetic field from 10 T to 30 T increases the neutron yield as shown in Fig. 150.3. Above 30 T, heat loss is ion diffusion dominated since radial electron conduction is essentially zero. Therefore, there is no further benefit from increasing the initial field. The magnetic field required to suppress ion heat flow introduces too much magnetic-field pressure, making it difficult to compress the target.

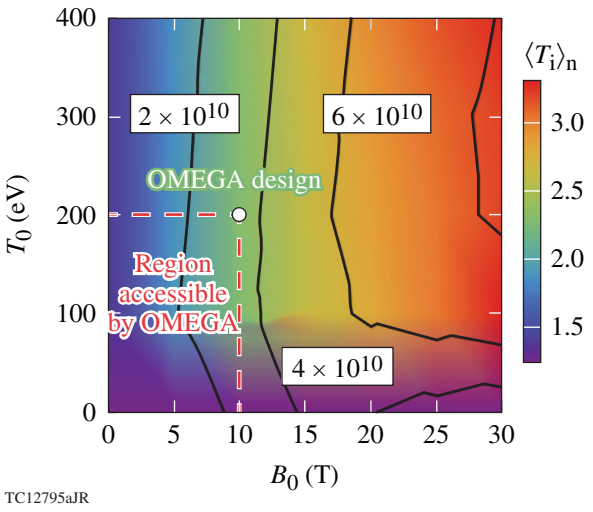

Figure 150.3
Neutron yields (contours) and neutron-averaged ion temperatures (colors) plotted as a function of initial axial magnetic field and preheat temperature. The region currently accessible by OMEGA is shown enclosed in the dashed lines.

Preheat Experiments

The focused preheat experiments determined the laser entrance hole (LEH) window transmission, backscatter, and sidescatter; a gas-filled cylindrical target was illuminated with up to 200 J of 3ω light in a 2.5-ns square-shaped pulse to study gas preheating *in situ*. The beam was focused on the LEH window and a 200-μm phase plate with smoothing by spectral dispersion and distributed polarization rotators were used. To study the window behavior in detail, window-only assemblies that consisted of the same 1.84-μm-thick polyimide foils used for the gas cylinder targets were studied. Using calorimeters, Raman and Brillouin spectrometers in different ports around the laser axis, soft x-ray emission from the LEH window and the gas, and optical emission from the surface of the gas-filled cylinder, we characterized the LEH window disassembly and the energy that propagates into the gas and determined a lower bound on the preheat temperature.

From the calorimeter measurements and backscatter diagnostics of the window-only shots, we determined that 64.5±2.0% of the laser energy incident on the LEH window is transmitted, with only 0.72±0.22% scattered outside of a 28° cone and 0.59±0.16% backscattered. It should be noted that the backscatter measurements herein are Brillouin measurements since the Raman measurement was below detectable threshold. We can then infer that 34±2.0% of the laser energy is absorbed in the window material as it disassembles. We have calculated the absorbed fraction using the 2-D hydrocodes *DRACO* and *FLASH*,[7] both of which give an absorbed energy of ~30%. Furthermore, we can post-process the output from these hydrocodes to model the soft x-ray spectra of the LEH window disassembly. The results of this spectral analysis compared directly to measurements from an array of differentially filtered x-ray diodes are in good agreement, as illustrated in Fig. 150.4.

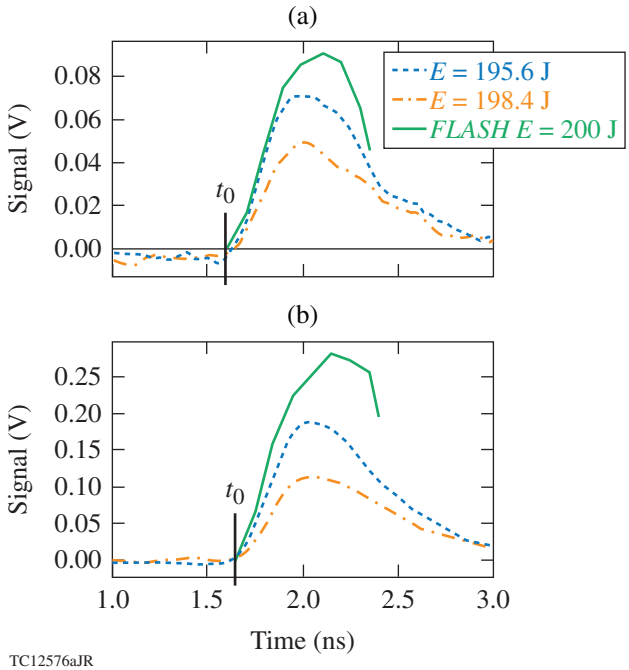

Figure 150.4
[(a), (b)] Two examples of the x-ray diode traces from experiments using a single laser beam and a laser entrance hole window assembly. The post-processed results from the *FLASH* hydrocode are in good agreement relative to the shot-to-shot variations.

Analysis of soft x rays from a diagnostic side window in the gas-filled cylindrical targets infer that a minimum possible gas temperature of 100 eV was achieved 1.3 ns into the laser pulse. This minimum value is determined from one shot, with other shots showing solutions above this minimum temperature. A parylene-AF4 fluorinated plastic cylinder was filled with 2-at. % neon-doped deuterium gas. The gas was then heated using the same laser beam that illuminated the LEH window assemblies. A side-on diagnostic window was imaged using a differentially filtered three-channel soft x-ray imager (SXR). Since the SXR is not absolutely calibrated and we have limited spectral information, the ratios of the spatially integrated channel signals are compared to a grid of possible temperatures and densities for the gas and the wall generated by a simulation. Comparing the channel ratios with this grid gives an infinite set of solutions, but if we constrain the solution space by insisting that the wall temperature cannot exceed the gas temperature, we establish the lowest possible value of the gas temperature to be 100 eV (shown in Fig. 150.5). Unfortunately, because of the limited dynamic range of the SXR and the quick increase in emission from increasing T_{gas}, temperatures above this 100-eV lower limit cannot be determined. We also obtain information about the gas heating from the x-ray diode array by looking at the LEH region. Much of the data is heavily encoded because of spectral integration, so we will rely primarily on comparison with hydrocodes to get a good idea of the heating process of the gas. A more-detailed paper on this experiment is expected to be submitted to Physics of Plasmas in the near future.

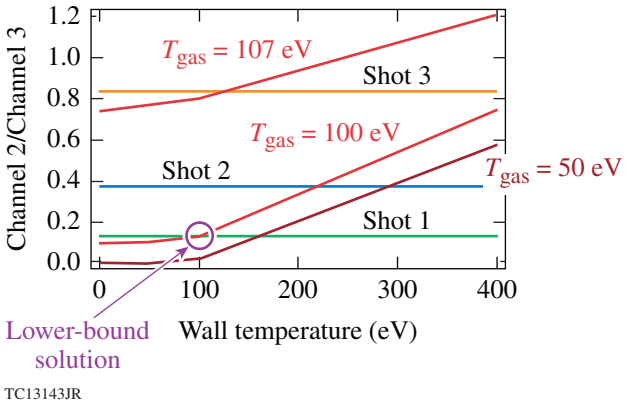

Figure 150.5
The ratio of Channel 2 to Channel 3 of the soft x-ray imager versus the wall temperature of the cylinder shows that the lower bound solution is 100 eV. Other solutions from different channel ratios either violate the condition of $T_{gas} > T_{wall}$ or give higher values.

Implosion Experiments

Implosion-only experiments were used to optimize the beam pointing and balance between normal and oblique beams; normal beams, referring to two rings of ten beams at an incidence angle of ±9°, and oblique beams, referring to two rings of ten beams at an incidence angle of ±31°. Both the separation and the intensity of the beams determine the uniformity and length of the cylindrical implosions. Using time-resolved x-ray images of the shell in flight, a shape can be determined by fitting the inner surface with a fourth-order polynomial function as shown in Fig. 150.6:

$$R(z) = a + b(z - z_0)^2 + c(z - z_0)^4. \quad (3)$$

The coefficients of this polynomial give a numerical measure that indicates if the shell has been overdriven at the ends or middle or uniformly imploded. Lineouts from time-integrated x-ray pinhole camera images also show the uniformity of the core and the length of the imploded region (as seen in Fig. 150.7). The illumination pattern that gives the most-uniform implosion empirically is an overlap of the oblique-angled beams at the center with the normal beams at the end and a reduction in energy of the normal beams to 83% of the maximum energy of the oblique beams. The result is the relatively uniform axial intensity profile shown in Fig. 150.8.

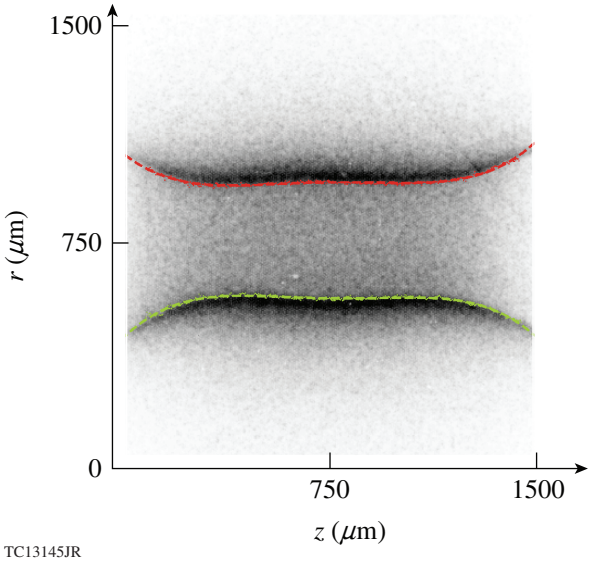

Figure 150.6
Each side of the shell was fit with a fourth-order polynomial to determine the shape of the shell in flight. The laser energy was then tuned to get the shape as flat as possible over the longest region.

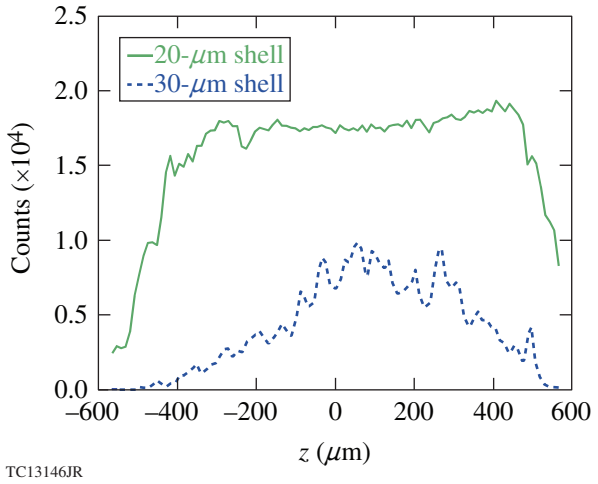

Figure 150.7
Thinner shells that have faster implosion velocities give broader and flatter emission from the core. A raw lineout of charge-injection device counts plotted versus the axial position from a pinhole camera demonstrates this fact. This suggests that a faster implosion is needed at the OMEGA scale to mitigate increased thermal losses. Pinhole images also provide a second metric for implosion uniformity.

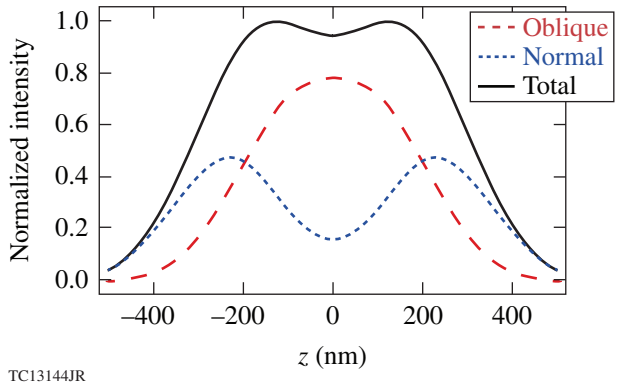

Figure 150.8
The irradiation pattern that gives the most cylindrically uniform compression.

Integrated MagLIF Experiments

The first integrated MagLIF experiments on OMEGA were used to scan preheat beam timing relative to the drive beams. Simulations and experiments both indicate the optimal time to fire the preheat laser was ~1.0 ns before the start of the drive beams, which corresponds to preheat finishing as the shell starts to implode. This made it possible for preheat to occur without introducing too much mix of wall material into the gas. Three times were scanned and the results can be seen in Fig. 150.9.

Yield enhancement from both preheat and magnetic field and preheat only matched with 1-D and 2-D simulation predictions based on the point design.[5] We have many shots with just the implosion from the beam-balancing campaign. In Fig. 150.10, the three best-quality implosion-only targets are shown along with a preheat and implosion shot, the two successful integrated MagLIF shots from the preheat beam-timing campaign, and the predicted performance of the point design from 2-D *HYDRA* MHD simulations. An implosion with magnetic field and no preheat has yet to be successfully completed. One- and two-dimensional MHD simulations replicating the implosion dynamics and magnetic-field compression are also under development. This is the first demonstration of yield enhancement in a magnetized cylindrical implosion

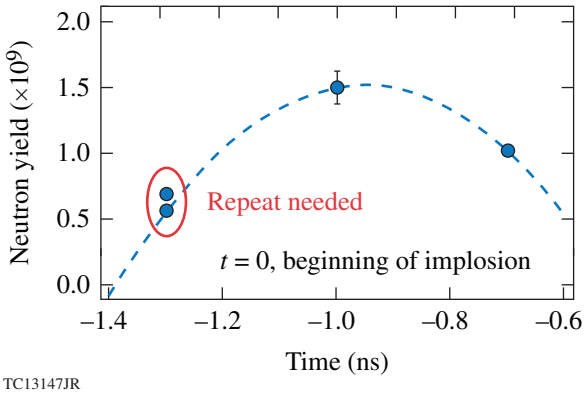

Figure 150.9
Neutron yield as a function of preheat beam time. The start of the drive beams is at $t = 0$. Some implosion beams were partially obstructed by the magnetic-field coils for both cases at the –1.3-ns timing, so these shots must be repeated, but the data follow the expected trend predicted by the simulations.

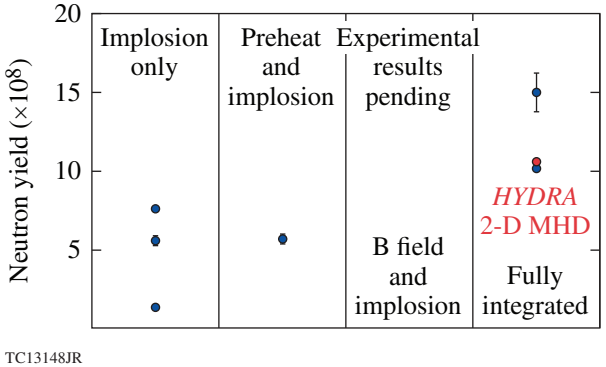

Figure 150.10
A summary of neutron yields for each configuration of the OMEGA MagLIF platform. Integrated MagLIF shots are compared to a 2-D magnetohydrodynamic (MHD) prediction made by the code *HYDRA*.

on OMEGA and is a very promising result that confirms the utility of laser-driven MagLIF in the development of a viable path toward ignition.

Future Work

At the time of publication of this article, the first experiments that will probe the evolution of the axial magnetic field will have been performed. Understanding the dynamics of the magnetic field within the fuel is directly related to the confidence interval of yield predictions from MHD simulations. If the magnetic-field advection within the gas is poorly understood, yields can vary in simulation by whole orders of magnitude. The dominant contribution to magnetic-field advection within the gas is from the Nernst effect,[8] which is an additional advection velocity to the magnetic field proportional to the electron heat flow.[9] Therefore, the heat flow itself can push against the magnetic field, thereby negating any benefit of the reduced thermal conduction. Proton radiography of the implosion can provide a direct indication of the rate of this additional advection.

Experiments to explore the MagLIF parameter space are scheduled to occur over the next year. A magnetic-field scan will explore the dependence on the magnetic field and help us understand the scaling of the Nernst effect with the magnetic field. A scan of the initial fuel density will determine the highest achievable convergence ratio before a decrease in performance. Laser-driven MagLIF has the ability to use thinner shells with higher implosion velocities than pulsed-power–driven MagLIF because of ablative stabilization of the Rayleigh–Taylor instability. A scan will be made to determine the minimum shell thickness that can be imploded without a significant decrease in neutron yield.

ACKNOWLEDGEMENT

The authors express their appreciation to the Mechanical Engineering Division of the Laboratory for Laser Energetics for the installation, characterization, and maintenance of the P9 3ω laser, which provides the preheating capabilities for mini-MagLIF. We also acknowledge the entire Omega Laser Facility, which continues to be a great asset for achieving experimental configuration milestones. The information, data, or work presented herein was funded in part by the Advanced Research Projects Agency-Energy (ARPA-E), U.S. Department of Energy, under Award Number DE-AR0000568. The views and opinions of authors expressed herein do not necessarily state or reflect those of the United States Government or any agency thereof. This material is based upon work supported by the Department of Energy National Nuclear Security Administration under Award Number DE-NA0001944.

REFERENCES

1. S. A. Slutz, M. C. Herrmann, R. A. Vesey, A. B. Sefkow, D. B. Sinars, D. C. Rovang, K. J. Peterson, and M. E. Cuneo, Phys. Plasmas **17**, 056303 (2010).

2. M. R. Gomez, S. A. Slutz, A. B. Sefkow, D. B. Sinars, K. D. Hahn, S. B. Hansen, E. C. Harding, P. F. Knapp, P. F. Schmit, C. A. Jennings, T. J. Awe, M. Geissel, D. C. Rovang, G. A. Chandler, G. W. Cooper, M. E. Cuneo, A. J. Harvey-Thompson, M. C. Herrmann, M. H. Hess, O. Johns, D. C. Lamppa, M. R. Martin, R. D. McBride, K. J. Peterson, J. L. Porter, G. K. Robertson, G. A. Rochau, C. L. Ruiz, M. E. Savage, I. C. Smith, W. A. Stygar, and R. A. Vesey, Phys. Rev. Lett. **113**, 155003 (2014).

3. J. P. Knauer, O. V. Gotchev, P. Y. Chang, D. D. Meyerhofer, O. Polomarov, R. Betti, J. A. Frenje, C. K. Li, M. J.-E. Manuel, R. D. Petrasso, J. R. Rygg, and F. H. Séguin, Phys. Plasmas **17**, 056318 (2010).

4. M. Hohenberger, P.-Y. Chang, G. Fiksel, J. P. Knauer, R. Betti, F. J. Marshall, D. D. Meyerhofer, F. H. Séguin, and R. D. Petrasso, Phys. Plasmas **19**, 056306 (2012).

5. J. R. Davies, D. H. Barnak, R. Betti, E. M. Campbell, P.-Y. Chang, A. B. Sefkow, K. J. Peterson, D. B. Sinars, and M. R. Weis, "Laser-Driven Magnetized Liner Inertial Fusion," to be published in Physics of Plasmas.

6. J. R. Davies, R. Betti, P.-Y. Chang, and G. Fiksel, Phys. Plasmas **22**, 112703 (2015).

7. B. Fryxell *et al*., Astrophys. J. Suppl. Ser. **131**, 273 (2000).

8. A. L. Velikovich, J. L. Giuliani, and S. T. Zalesak, in *2014 IEEE 41st International Conference on Plasma Sciences (ICOPS) held with 2014 IEEE International Conference on High-Power Particle Beams (BEAMS)* (IEEE, Washington, DC, 2014).

9. A. Nishiguchi *et al*., Phys. Rev. Lett. **53**, 262 (1984).